SRI International

(1)

Quarterly Technical Report 8 • 1 September 1994

IR MATERIALS PRODUCIBILITY

M.A. Berding, Sr. Research Physicist
A. Sher, Program Director
S. Krishnamurthy, Sr. Research Physicist
Physical Electronics Laboratory

SRI Project 3820

Prepared for:

Contracting Officer's Technical Representative
Advanced Research Projects Agency
Microelectronics Technology Office (MTO)
3701 N. Fairfax Drive
Arlington, VA 22203-1714

Attn: Mr. Raymond Balcerak

ARPA Order No. 8557; Program Code Nos. 2H20, 2D10

Contract MDA972-92-C-0053

Covering the period: 1 May through 31 August 1994

333 Ravenswood Ave • Menlo Park, CA 94025-3493

IR MATERIALS PRODUCIBILITY

M.A. Berding, Sr. Research Physicist
A. Sher, Program Director
S. Krishnamurthy, Sr. Research Physicist
Physical Electronics Laboratory

SRI Project 3820

SRI Project 3820

Prepared for:

Contracting Officer's Technical Representative
Advanced Research Projects Agency
Microelectronics Technology Office (MTO)
3701 N. Fairfax Drive
Arlington, VA 22203-1714

Attn: Mr. Raymond Balcerak

ARPA Order No. 8557; Program Code Nos. 2H20, 2D10

Contract MDA972-92-C-0053

Covering the period: 1 May through 31 August 1994

APPROVED FOR PUBLIC RELEASE
DISTRIBUTION UNLIMITED

Approved:

Eric Pearson, Director
Physical Electronics Laboratory

Donald L. Nielson, Vice President
Computing and Engineering Sciences Division

REPORT DOCUMENTATION PAGE

Form Approved
OMB No. 0704-0188

1. AGENCY USE ONLY (Leave Blank)	2. REPORT DATE	3. REPORT TYPE AND DATES COVERED
	1 September 1994	Quarterly Technical 8 (1 May to 31 Aug. 1994)

4. TITLE AND SUBTITLE

IR Materials Producibility

5. FUNDING NUMBERS

6. AUTHORS

M.A. Berding, A. Sher, S. Krishnamurthy

7. PERFORMING ORGANIZATION NAME(S) AND ADDRESS(ES)

SRI International
333 Ravenswood Avenue
Menlo Park, CA 94025-3493

8. PERFORMING ORGANIZATION REPORT NUMBER

9. SPONSORING/MONITORING AGENCY NAME(S) AND ADDRESS(ES

Advanced Research Projects Agency
Microelectronics Technology Office, Infrared Focal Plane Array Program
3701 North Fairfax Drive
Arlington, Virginia 22203-1714

10. SPONSORING/MONITORING AGENCY REPORT NUMBER

11. SUPPLEMENTARY NOTES

12a. DISTRIBUTION/AVAILABILITY STATEMENT

Approved for public release; distribution unlimited

12b. DISTRIBUTION CODE

13. ABSTRACT *(Maximum 200 words)*

The work summarized in this report covers the eighth quarter of a program with a goal that is threefold: first, to study the properties of native point defects in infrared focal-plane array (IRFPA) active and substrate materials; second, to study the properties of native point defects in two classes of photonic materials, the wide-gap II-VI compounds (ZnSe as the prototype for which impurity properties will also be calculated) and the nonlinear optical materials ($LiNbO_3$ as the prototype); the third, to study the properties of HgZnTe as a very-long-wave infrared (VLWIR) detector material. During the eighth quarter:

- We have continued the refinement of the calculation of the tellurium antisite-mercury vacancy pair in HgCdTe. We find a binding energy of more than 1 eV.
- We have developed a strategy for calculating the ionization energies of defects in semiconductors, and have tested the strategy on the arsenic antisite in GaAs with good results. We have begun the calculation of the ionization energies in CdTe and ZnSe, and preliminary results are reported.
- Transport-related properties have been calculated for HgCdTe and HgZnTe and compared with results using the effective mass approximation.

14. SUBJECT TERMS

native point defects; infrared devices photonic material; HgTe; CdTe; ZnSe; HgCdTe

15. NUMBER OF PAGES

25

16. PRICE CODE

17. SECURITY CLASSIFICATION OF REPORT	18. SECURITY CLASSIFICATION OF THIS PAGE	19. SECURITY CLASSIFICATION OF ABSTRACT	20. LIMITATION OF ABSTRACT
Unclassified	Unclassified	Unclassified	Unlimited

SUMMARY

The work summarized in this report covers the eighth quarter of a program with a goal that is threefold: first, to study the properties of native point defects in infrared focal–plane array (IRFPA) active and substrate materials; second, to study the properties of native point defects in two classes of photonic materials, the wide-gap II-VI compounds (ZnSe as the prototype for which impurity properties will also be calculated) and the nonlinear optical materials ($LiNbO_3$ as the prototype); and third to study the properties of HgZnTe as a very-long-wave infrared (VLWIR) detector material. During the eighth quarter:

- We have continued the refinement of the calculation of the tellurium antisite – mercury vacancy pair in HgCdTe. We find a binding energy of more than 1 eV.
- We have developed a strategy for calculating the ionization energies of defects in semiconductors, and have tested the strategy on the arsenic antisite in GaAs with good results We have begun the calculation of the ionization energies in CdTe and ZnSe, and preliminary results are reported.
- Transport-related properties have been calculated for HgCdTe and HgZnTe and compared with results using the effective mass approximation.

1. NATIVE POINT DEFECTS IN HgCdTe AND RELATED IR MATERIALS

We have calculated the binding energy for the tellurium antisite mercury vacancy pair, corresponding to the reaction

$$V_{Hg} + Te_{Hg} \rightarrow (V_{Hg}Te_{Hg})_{Pair}. \quad (1)$$

where V_{Hg} and Te_{Hg} are the isolated mercury vacancy and tellurium antisite point defects and $(V_{Hg}Te_{Hg})_{Pair}$ is the bound mercury vacancy tellurium antisite pair in which the point defects reside on adjacent cation sites. We expected this pair to be important for two reasons. First, both the mercury vacancy and the tellurium antisite are important defects in $Hg_{0.78}Cd_{0.22}Te$ and as isolated species are present in significant quantities. Second, the mercury vacancy is an acceptor and the tellurium antisite is a donor, and therefore a Coulomb attraction will contribute to their binding. Finally, the tellurium antisite produces a compressive strain and the mercury vacancy produces a tensile strain (although somewhat smaller in magnitude than that of the antisite), and therefore there will be a mechanical attraction between the point defects.

The binding energy of the pair was calculated using the self-consistent full potential linearized muffin–tin orbital (FP-LMTO) method and supercells discussed in previous quarterly reports. We have completed the calculation using the 32-atom supercell for both the isolated defects and the defect pair and with a minimal basis set, and we obtained a binding energy of 1.1 eV. We are currently completing the calculations with a larger basis set size and with a larger supercell. These calculations are extremely computationally intensive, and strategies to expedite the calculations are being developed.

We have generalized our previously developed quasichemical method to include defect complexes. We are currently completing a preliminary analysis of the density of this defect pair we expect in $Hg_{0.78}Cd_{0.22}Te$. We are also completing the analysis of this defect in light of the fact that the tellurium antisite is likely to be a slow diffuser, and therefore may not reach equilibrium either as an isolated defect or as a part of a defect complex. Defects of this analysis will be presented in the next quarterly report.

2. CALCULATION OF IONIZATION ENERGIES

An important part of our calculation of defect densities in semiconductors (HgCdTe, ZnSe, HgZnTe, and CdTe) is the determination of the ionization energies. In HgCdTe, we used a rather crude analysis to determine whether the native point defects were donors or acceptors because our calculations of the densities of the defects were relatively insensitive to the exact determination of the ionization energies. Unfortunately, this crude analysis does not yield the exact position of the levels in the gap for either the first or second ionization levels, nor does it indicate whether a defect is a negative-U center. For the wider-gap semiconductors such as CdTe and ZnSe, the locations of the levels in the gap are much more important and will significantly impact the densities of the defects. Thus, we are working towards a method to better locate the defect levels in the gap. Much of the work this quarter has been focused on this task, and is summarized below.

We assume that the total energy of a solid is a smooth function of the system charge, z, that is

$$E(Z) = E_0 + E_1 z + E_2 z^2. \tag{2}$$

The energy per electron to change the system charge from z_1 to z_2 is to lowest order given by

$$E_{ion}(z_2, z_1) = \frac{E(z_2) - E(z_1)}{z_2 - z_1} = E_1 + E_2(z_2 - z_1). \tag{3}$$

If z_1 and z_2 are integers differing by unity, E_{ion} is just the ionization energy. Note that

$$\left(\frac{\partial E}{\partial z}\right)_{\frac{z_2+z_1}{2}} = E_1 + E_2(z_2 - z_1). \tag{4}$$

Now for an infinite system, the change in energy when an electron is added or removed from the system is the Fermi energy or electron chemical potential ϵ_F so that

$$E_{ion}(z_2, z_1) = \left(\frac{z_2 + z_1}{2}\right)\epsilon_F. \tag{5}$$

We are interested in the one–electron ionization levels of defects, that is, the energy of the levels with respect to the band edges. We will always take the energies with respect to the valence band edge due to the local density approximation (LDA) band-gap errors (consequences of which on the defect levels are to be discussed further

below). For the one-electron levels we take the difference between the Fermi level for the half-filled state and the energy of top of the valence band, ϵ_v, that is

$$E_d(1) = \epsilon_F(z = -0.5) - \epsilon_v \tag{6}$$

$$E_d(2) = \epsilon_F(z = -1.5) - \epsilon_v \tag{7}$$

for the first and second ionization levels of a donor and

$$E_a(1) = \epsilon_c - \epsilon_F(z = +0.5) \tag{8}$$

$$E_a(2) = \epsilon_c - \epsilon_F(z = +1.5) \tag{9}$$

for the first and second ionization levels of an acceptor. Here ϵ_F is the zero-temperature Fermi level of the system with a nondegenerate density of a single defect species, ϵ_v is taken from the bulk calculation, and ϵ_c is determined from $\epsilon_v + E_{gap}^{experiment}$. Because the zero of energy is arbitrary in the LDA calculations, we have assured a proper alignment of the bands (and consequently the Fermi energies) by aligning bulk-like characteristic features in the density of states of the bulk and defect calculations.

We have corrected for the finite width of the gap state in the following manner. We know that in the limit of very large systems the gap states will be very narrow, approaching a delta function, and will accept two electrons per defect for s-like (or A1-symmetry) states and six electrons for p-like (or T2-symmetry) states. Because we are doing supercell calculations, our localized levels in the gap are quite broad because of the overlap of the wave functions of point defects in adjacent supercells. We correct for this finite width by associating the ionization energy level with the center of gravity of this localized level (as determined from the density of states).

2.1 NATIVE POINT DEFECTS IN CdTe

We applied the analysis discussed above to determine the energy levels of native point defect in CdTe. Table 1 presents our preliminary results for CdTe.

A preliminary analysis of the density of the native point defects, including both neutral and ionized states, has been completed. We find that in equilibrium, the cadmium vacancy and the tellurium antisite dominate at low cadmium pressures, while the cadmium vacancy and the cadmium interstitial dominate at the higher cadmium pressures. A more complete analysis will be presented in the next quarterly report.

Table 1. Ionization energies for the native point defects in CdTe. Results are from LMTO calculations using the atomic-spheres approximation, and do not include Jahn-Teller distortions.

Defect	Acceptor levels		Donor levels	
	single	double	single	double
V_{Cd}	0.	0.10		
V_{Te}			0.70	0.85
Cd_{Te}	1.30	1.40		
Te_{Cd}			0.18	0.33
$Cd_{I_{Cd}}$			0.73	1.00
$Cd_{I_{Te}}$			0.34	0.56
$Te_{I_{Cd}}$			0.93	1.20
$Te_{I_{Te}}$			0.55	0.84

2.2 NATIVE POINT DEFECTS IN ZnSe

We are still completing the calculation of the ionization energies of the native point defect in ZnSe. Although we have not yet completed the ionization energy calculation, we have demonstrated that equilibrium native defects can compensate the p-type dopants in ZnSe.

Figure 1 shows the neutral native point defects in ZnSe at 600 °C as a function of zinc partial pressure. The zinc vacancy is the dominant defect followed by the selenium vacancy at high zinc pressures and the selenium antisite at low zinc pressures. From our calculations to date, the zinc vacancy appears to be an acceptor, while both the selenium antisite and vacancy appear to be donors.

To demonstrate the p-type compensation mechanism, we consider two cases. First we assume that the zinc vacancy has a single acceptor level at midgap, while the selenium vacancy and antisites are assumed to be double donors with their first ionization level at the conduction band edge, and the second level at 0.1 eV. Using these ionization levels and the defect formation energies from our completed calculations for the neutral defects (used to generate Figure 1), we have completed a defect analysis at 600 °C with just these three defects. We find that the material can be easily doped n-type throughout the phase stability region, but a high level of p-type doping cannot be achieved. This situation is illustrated in Figure 2, where we have completed our calculations of the defect concentrations for an impurity concentration of 10^{19} cm−3.

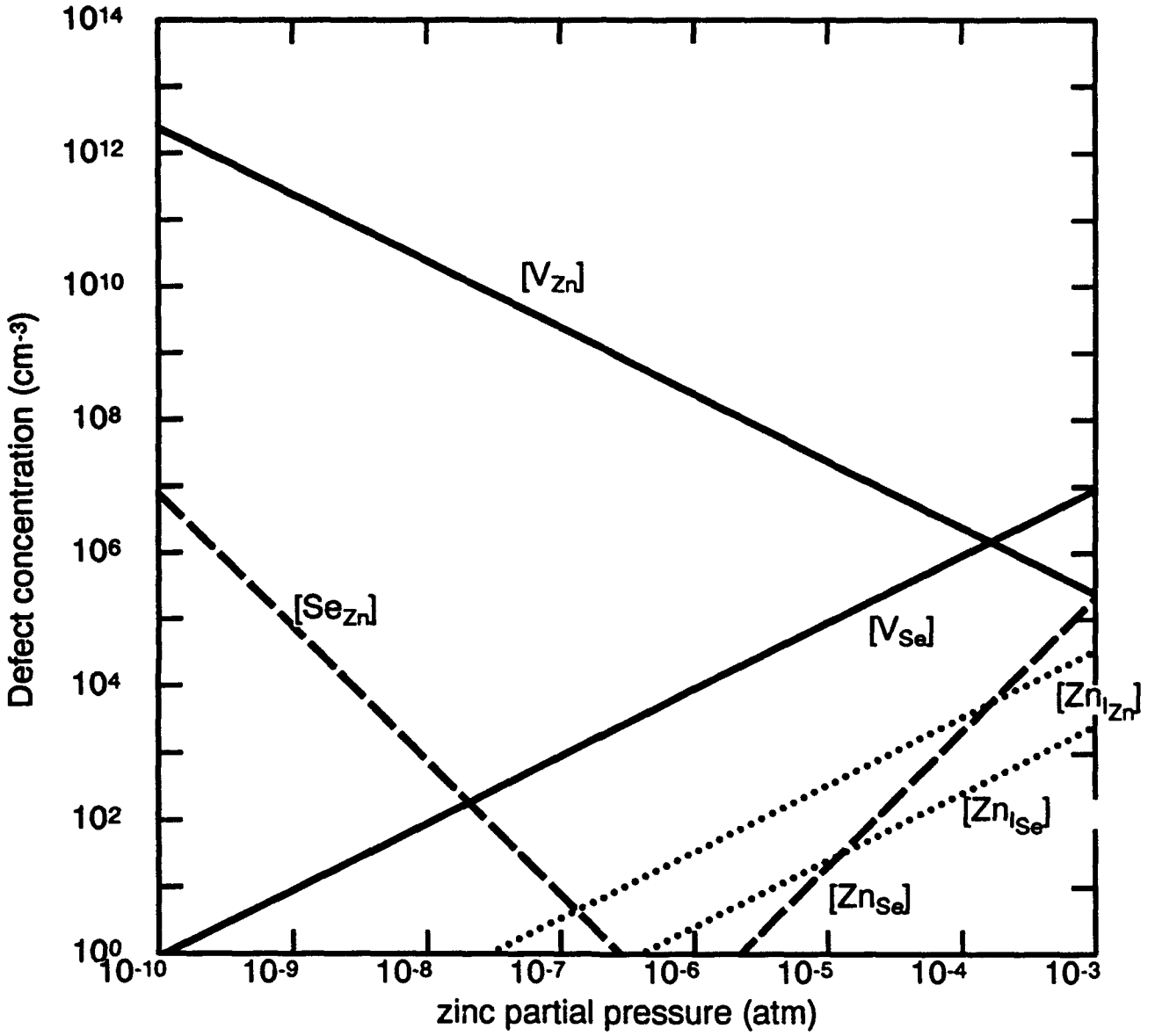

Figure 1 Neutral native point defect concentrations ZnSe at 600°C

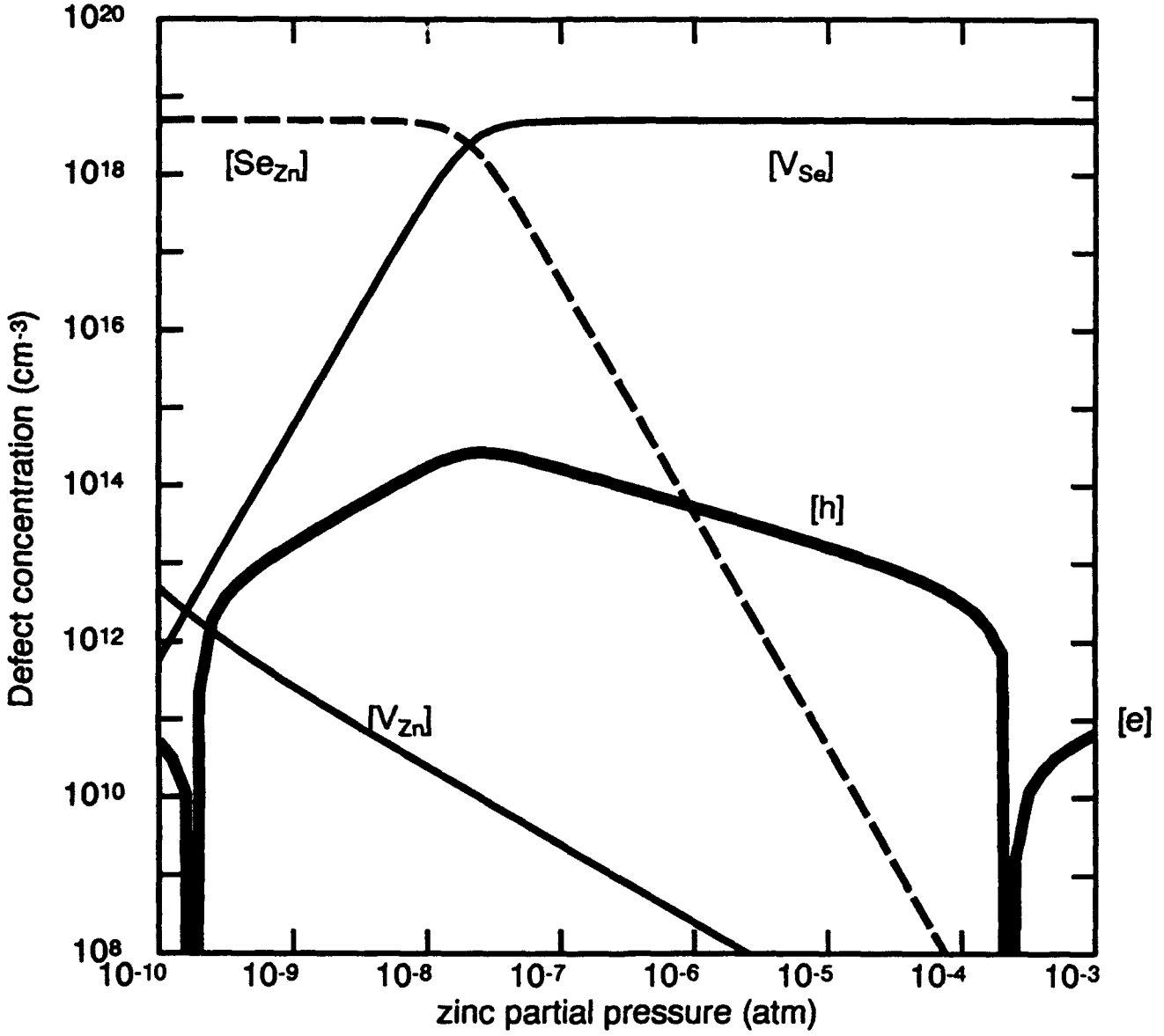

(a) with 10^{19} cm^{-3} acceptor impurities

Figure 2 Total native point defect concentrations (neutral and ionized) in ZnSe, which is equilibrated at 600°C assuming V_{Se} and Se_{Zn} are shallow donors and V_{Zn} is a deep acceptor. Electronic equilibration at room temperature

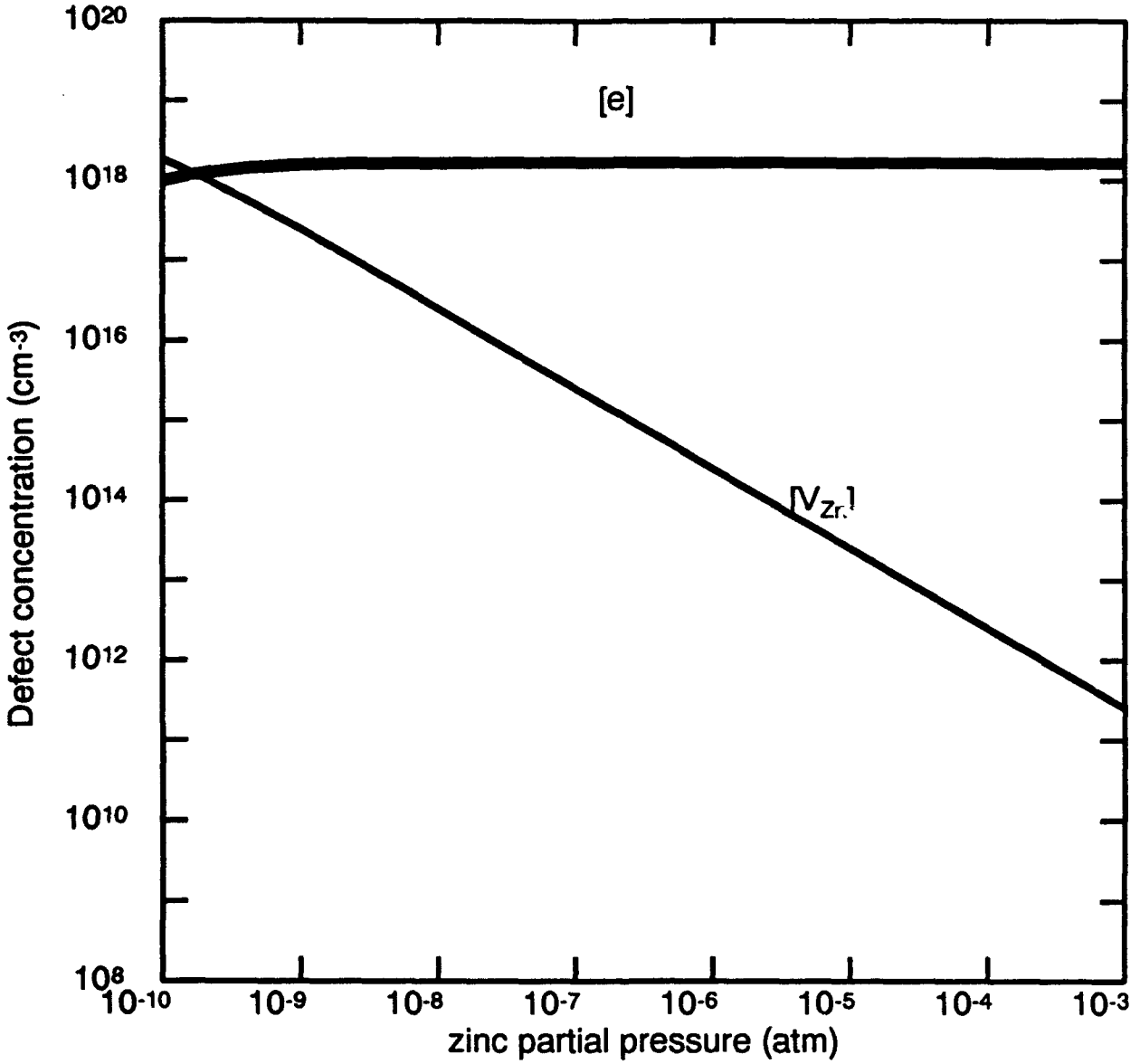

(b) with 10^{19} cm^{-3} donor impurities

Figure 2 (continued)

Next, we have considered the case in which the zinc vacancy has associated with it two acceptor levels at 0 and 0.1 eV, while the selenium antisite and vacancy are assumed to have singly ionizable midgap levels. Results for p- and n-type impurity concentrations of 10^{19} cm^{-3} are illustrated in Figure 3. As one can see in this case, the material is easily doped p-type but cannot be doped n-type.

Obviously the presence of self-compensation in ZnSe depends on the true position of the ionization levels in the gap. Our preliminary results indicate that neither of the extreme limits discussed above will be valid. Our present results indicate that the acceptor level associated with the zinc vacancy will be relatively shallow, and because of the dominance of the neutral zinc vacancy (Figure 1), we expect that this defect will be the major player in the compensation game. Thus, at this point we expect that the native point defects are not responsible for the self-compensation mechanism in ZnSe.

When our native point defect analysis is complete, we will begin to examine issues related to the dark line defects in ZnSe, their relationship to the stacking faults, and means for their elimination and/or passivation.

3. HgZnTe AS AN LWIR DETECTOR MATERIAL

The transport-related properties such as electron mobility, Hall coefficient, and Fermi levels are calculated with accurate analytical band structures, Fermi-Dirac (FD) statistics and experimental energy gap. Thus, calculated values differ substantially from the ones obtained with effective mass or parabolic band structure approximation of $Hg_{0.73}Zn_{0.17}Te$ alloy. We find that approximating the Hall factor by unity over a wide range of carrier concentrations is accurate only for temperatures less than 100 K. An error of about 50% is expected at higher temperatures and low carrier concentration (10^{15} cm^{-3}), and about 20% is expected at low T and high carrier concentration (10^{18} cm^{-3}). The impurity, phonon and alloy disorder-limited mobility calculations with full solution to Boltzmann transport equation with FD statistics predict a hump near 40 K. The mobility in HgZnTe is about 10-20% higher than that in HgCdTe.

3.1 INTRODUCTION

The experimental results on electron transport properties of semiconductors is often compared to theory that rests on three approximations, namely, parabolic band

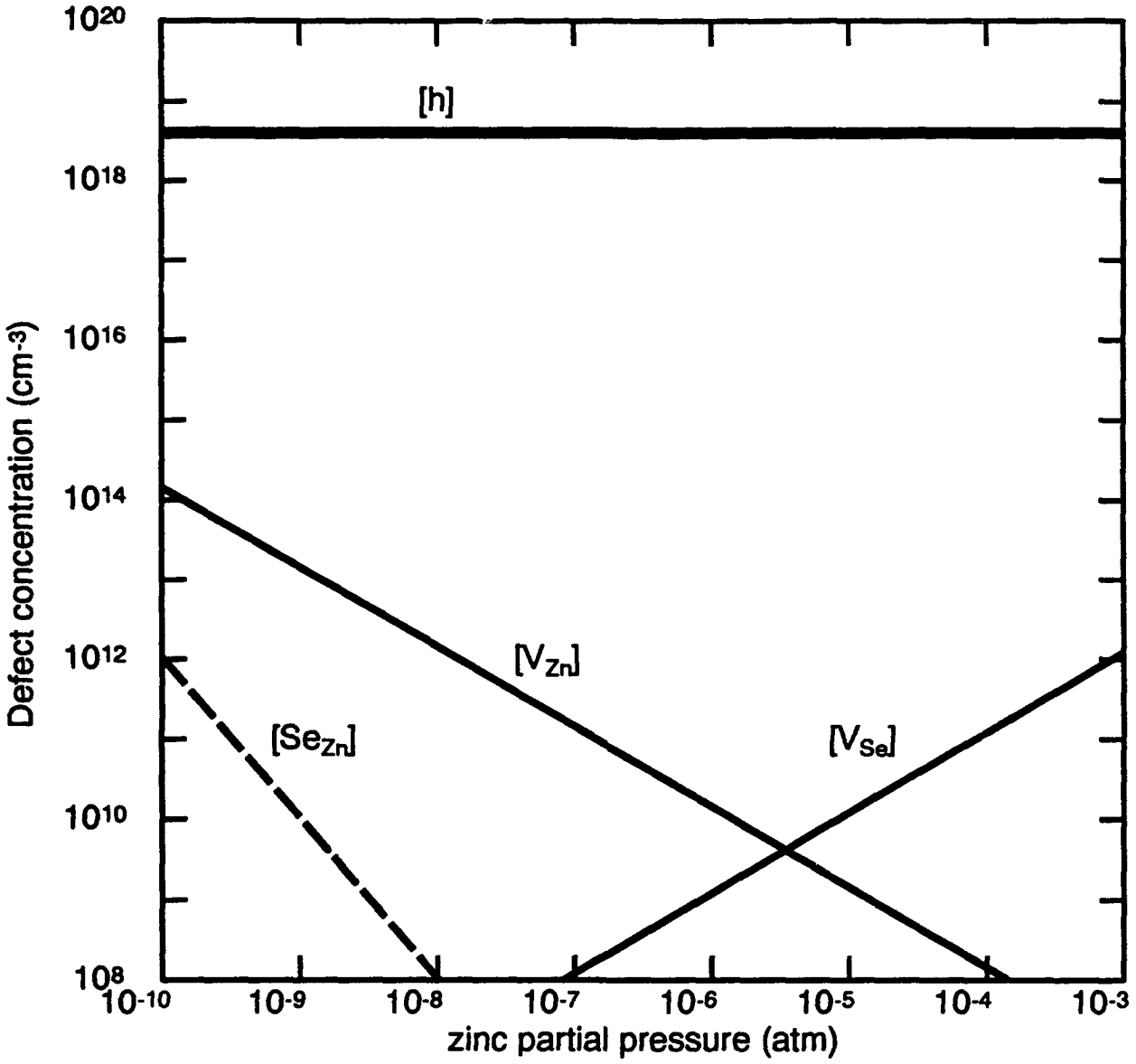

(a) with 10^{19} cm^{-3} acceptor impurities

Figure 3 Total native point defect concentrations (neutral and ionized) ZnSe which is equilibrated at 600° assuming V_{Se} and Se_{Zn} are deep donors and V_{Zn} is a shallow acceptor. Electronic equilibration at room temperature

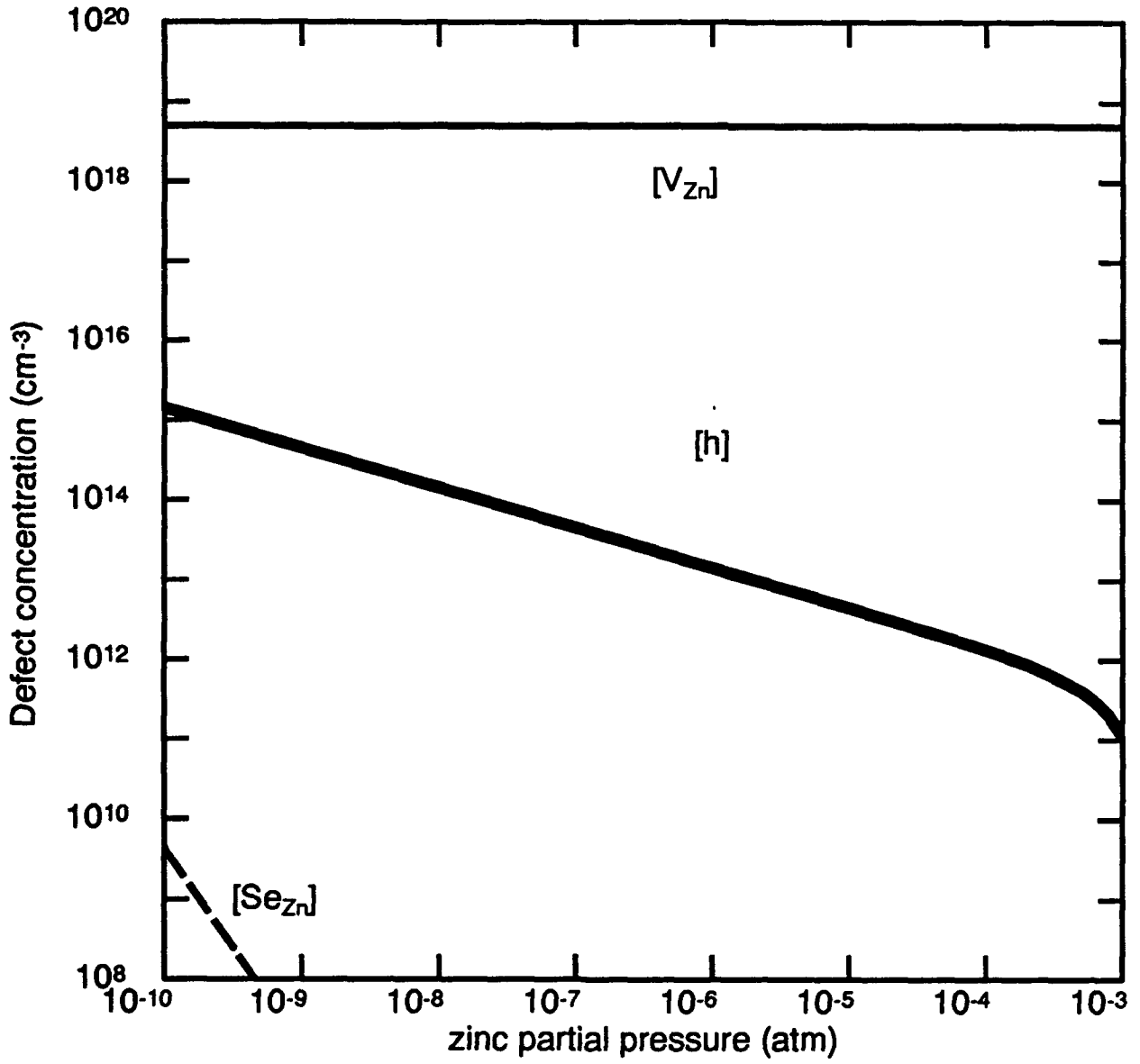

(b) with 10^{19} cm^{-3} donor impurities

Figure 3 (continued)

structures for those states occupied in the measurement, Maxwell-Boltzmann (MB) statistics, and collision time approximation to the full Boltzmann gain-loss equation. These approximations are made to all scattering mechanisms whether they are elastic or inelastic. It is well known that, even in large-gap materials, the constant effective mass approximation is valid only very near ($\approx E_g/10$) to the band edge (Kane, 1957; Krishnamurthy et al., 1987). This approximation has been recognized to be particularly poor for narrow-gap materials, and nonparabolic corrections calculated in the **k.p** formalism are often used (Schmidt 1970, Meyer and Bartoli, 1982; Bartoli et al., 1982). This correction is substantial but still differs considerably from our more accurately calculated band structures. In addition, our fit of the conduction band to an analytical function makes many results transparent and simplifies the calculations. As the Fermi energy can easily move into the conduction band of lightly doped small-gap materials, the form of the Boltzmann equation with FD (instead of the usual MB) statistics must be used to obtain accurate transport coefficients.

Here we report results from our study of absorption coefficient, Fermi energy, Hall coefficient, and electron mobility calculated with FD statistics and accurate pseudopotential band structures fine tuned with tight-binding (TB) corrections.

3.2 BAND STRUCTURE

Quantitatively accurate band structures of group IV elements (Krishnamurthy et al., 1986), III-V compounds (Chen and Sher, 1981), and II-VI compounds (Chen and Sher, 1981; Berding et al., 1987) can be obtained using a minimum set of sp^3 orbitals in semiempirical calculations. First, empirical pseudopotential form factors are used to calculate a TB Hamiltonian H in the minimum set. H is then transformed into a zeroth-order H_0 in an orthonormal basis. Then, a perturbative Hamiltonian having a first-neighbor TB form is added to H_0 to fine tune the band structure. Because long-range interactions are included in this Hamiltonian, the measured band curvatures are correctly reproduced. This procedure is followed for both HgTe and CdTe, and then the alloy band structures are calculated in the coherent potential approximation.

We focus $Hg_{0.22}Cd_{0.78}Te$ alloy with 100-meV band gap for the studies reported here. We find that the calculated conduction band is replicated very well by a hyperbola,

$$E_k = \left(\gamma k^2 + c^2\right)^{1/2} - c \tag{10}$$

where γ and c are adjusted to fit the calculated band structure in the energy range of interest. When γ and c are treated as constants related to the band gap E_g and the effective mass, this expression will reduce to the same nonparabolic correction form obtained in the k·p method. Our values of γ and c are 47.78 and 0.058, respectively, whereas the corresponding k·p values are 36.0 and 0.05. The differences are found to be large enough to cause a noticeable change in the band structure. The band structure calculated by diagonalizing the Hamiltonian is shown in Figure 1 (thick line). We find that our hyperbola fits the band structure calculated by diagonalizing the Hamiltonian quite well up to an energy of 0.5 eV from the conduction band edge. Without loss of accuracy, in the studies considered here, Eq. (10) is used as the energy dispersion relation in transport expressions that follow.

For energies $E - E_c$ greater than 50 meV where the shape of the conduction band is nearly linear in k, the group velocity is a constant independent of the k. Then the density of states (DOS) increases proportional to E rather than $E^{1/2}$ as in the case of parabolic bands. Clearly, these features modify the transport properties of electrons occupying these states. As we will show in the following section, at the carrier concentration and temperatures often found in device structures, the Fermi level falls into the region where these features contribute.

3.3 FERMI LEVEL

The calculation of Fermi level $\epsilon_F$as a function temperature T and doping concentration n_D is required for all transport calculations. A knowledge of temperature-dependent gap E_g(T) is essential to obtain ϵ_F. Ideally, temperature dependence should be included in the Hamiltonian from which the variation of E_g with T could be obtained. We have developed a general method to incorporate phonon effects on the band gap. However, we have used the experimental values (Sher et al., 1986) of the gap. After studying the effects of various approximations and obtaining trends, the calculations will be repeated with temperature-dependent Hamiltonian.

Then, the $\epsilon_F$is calculated from the condition (Sze, 1981) that at a given T the number electrons in the conduction band is the sum of electrons excited from the valence band and donor levels. In this study where the modifications caused by the band structures are being emphasized, the donor states are assumed to be located at the bottom of the conduction band. The valence and conduction band DOS are calculated from our band structure. The valence band DOS yields a hole effective mass of 0.65. The ϵ_F(measured from valence band edge) as a function of T and n_D

calculated from hyperbolic band structures are given in Figure 4. Hyperbolic band makes substantial change from parabolic band generated values.

3.4 HALL COEFFICIENT

The carrier density, n in n-type material is normally deduced from measurements of Hall coefficient R_H, given by r_e/en, by assuming the Hall factor r_e is unity. If one uses parabolic approximation and MB statistics, r_e is approximately unity. We set out to examining the effect of removing these approximations using the correct band structures. It requires generalizing the Boltzmann transport equation (BTE) to include FD distribution function. We have

$$\frac{df(\mathrm{k})}{dt} = \sum_{\mathrm{k}'} [w(\mathrm{k},\mathrm{k}')f(\mathrm{k}')(1-f(\mathrm{k})) - w(\mathrm{k}',\mathrm{k})f(\mathrm{k})(1-f(\mathrm{k}'))] \tag{11}$$

The first term of the right-hand side is the gain term, and the second term is the loss term. In equilibrium, the left-hand side of Eq. (11) is identically zero and f becomes the equilibrium FD distribution function f_0, given by

$$f_0(E_k) = \left(e^{\beta(E_k-\epsilon_F)}+1\right)^{-1} \tag{12}$$

where β is $(k_B T)^{-1}$. In the presence of electric and magnetic field,

$$\frac{df(\mathrm{k})}{dt} = \frac{\partial f(\mathrm{k})}{\partial t} + \nabla f(\mathrm{k}) \cdot \frac{e}{\hbar}(E + v \times B) \tag{13}$$

In steady state, the $\partial f(\mathrm{k})/\partial t$ in Eq. (13) vanishes. In the small field regime, we can linearize f and write it as a sum of f_0 and a perturbation $f_1(\mathrm{k})$. Disregarding the derivative of $f_1(\mathrm{k})$ and after some algebraic manipulation, Eq. (13) reduces to,

$$\nabla f_0(\mathrm{k}) \cdot \frac{e}{\hbar}(\mathbf{E} + \mathbf{v} \times \mathbf{B}) = \sum_{\mathrm{k}'} [\mathbf{W}(\mathrm{k},\mathrm{k}')f_1(\mathrm{k}') - \mathbf{W}(\mathrm{k}',\mathrm{k})f_1(\mathrm{k})] \tag{14}$$

where the renormalized **W** and the usual transition probability per unit time w are related by

$$\mathbf{W}(\mathrm{k},\mathrm{k}') = w(\mathrm{k},\mathrm{k}')\frac{(1-f_0(\mathrm{k}))}{(1-f_0(\mathrm{k}'))} \tag{15}$$

Note that for elastic scattering **W** and w are equal. However, for inelastic cases the effect depends on whether energies at k and k' are larger or smaller than ϵ_F. If both initial and final energies are larger (or smaller) than ϵ_F, only a small correction

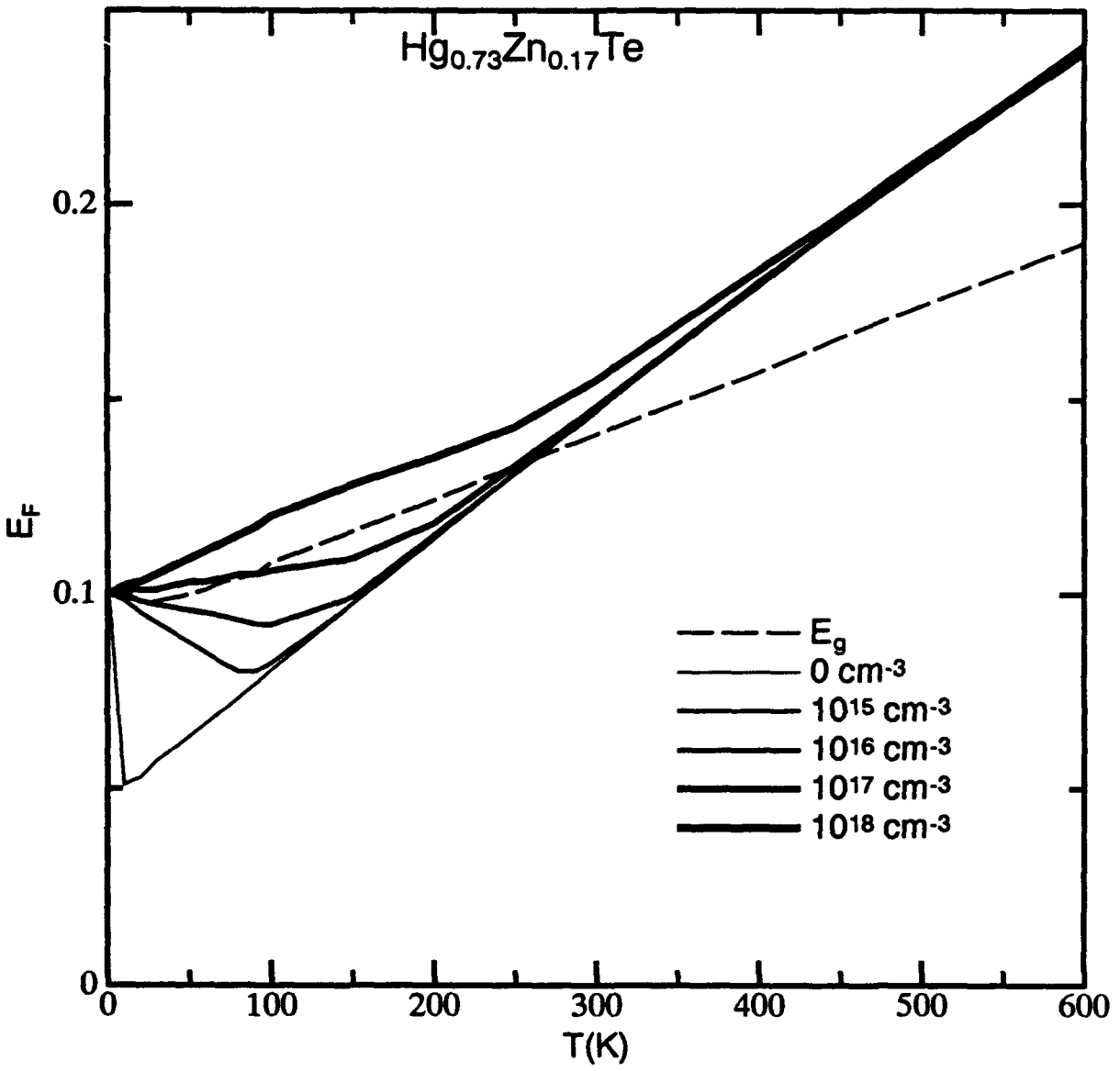

Figure 4 Fermi energy as a function of temperature: HgZnTe

to w is expected. However, if the initial state is above $\epsilon_F$and the final state is below ϵ_F, that scattering is suppressed.

In the collision time approximation, the gain term in Eq. (15) is neglected and the effective collision time $\tau_{\mathbf{k}}^F$ is

$$(\tau_{\mathbf{k}}^F)^{-1} = \sum_{\mathbf{k}'} \mathrm{W}(\mathbf{k}', \mathbf{k}) \tag{16}$$

Using this collision time approximation, it is straightforward to obtain the expression for r_e:

$$r_e = 3k_B T \left[\frac{\sum_{\mathbf{k}} f_0 \sum_{\mathbf{k}} k^2 \gamma_{\mathbf{k}}^3 (\tau_{\mathbf{k}}^F)^2 f_0(1-f_0)}{(\sum_{\mathbf{k}} k^2 \gamma_{\mathbf{k}}^2 \tau_{\mathbf{k}}^F f_0(1-f_0))^2} \right] \tag{17}$$

where $\nabla_{\mathbf{k}} E_k$ is $\gamma_{\mathbf{k}}$ k. The calculated r_e with hyperbolic band structures is shown for various T and doping densities in Figure 5. The r_e is approximately 1 for lower temperatures. However, at higher temperatures, it shows considerable structure with a maximum value of about 1.6. The ratio of r_e calculated with hyperbolic bands to that obtained with parabolic bands is shown in Figure 6. Our calculations show that parabolic values can be in error by as much as 50%. The experimentalists normally use a value of 1 for r_e in deducing the intrinsic density from Hall measurements, suggesting that reported values may be smaller by as much as 50% at intermediate temperatures.

3.5 DRIFT MOBILITY

The formalism developed above to find the solution to BTE with FD statistics can be used to calculate the mobility μ. We obtain the following expression in collision time approximation:

$$\mu = \frac{e}{3\hbar^2 k_B T} \left[\frac{\sum_{\mathbf{k}} k^2 \gamma_{\mathbf{k}}^2 \tau_{\mathbf{k}}^F f_0(1-f_0)}{\sum_{\mathbf{k}} f_0} \right] \tag{18}$$

The calculated mobility by including the scattering due to ionized impurities and polar optic phonons as a function of temperature and doping density, is shown in Figure 7. The change in the Debye screening length, complicated variation of Fermi level, and phonon scattering give rise to a crossover in mobility near 40 K, as seen in Figure 7. However, it is well known that the collision time approximation always overestimates the velocity transition rate that determines the mobility. For meaningful comparison with experiment, we generalized the above procedure to get full

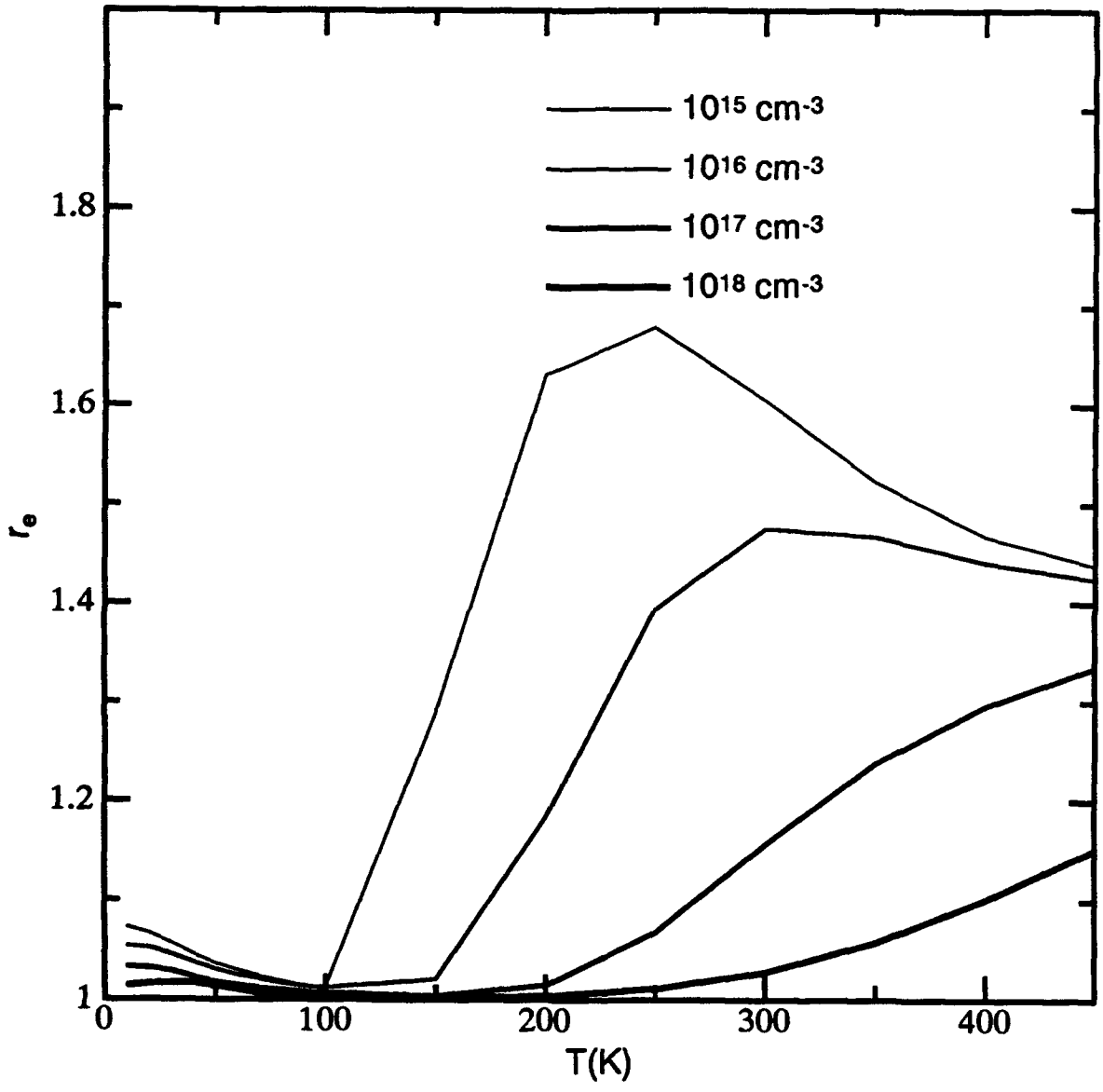

Figure 5 Hall factor as a function of temperature: HgZnTe

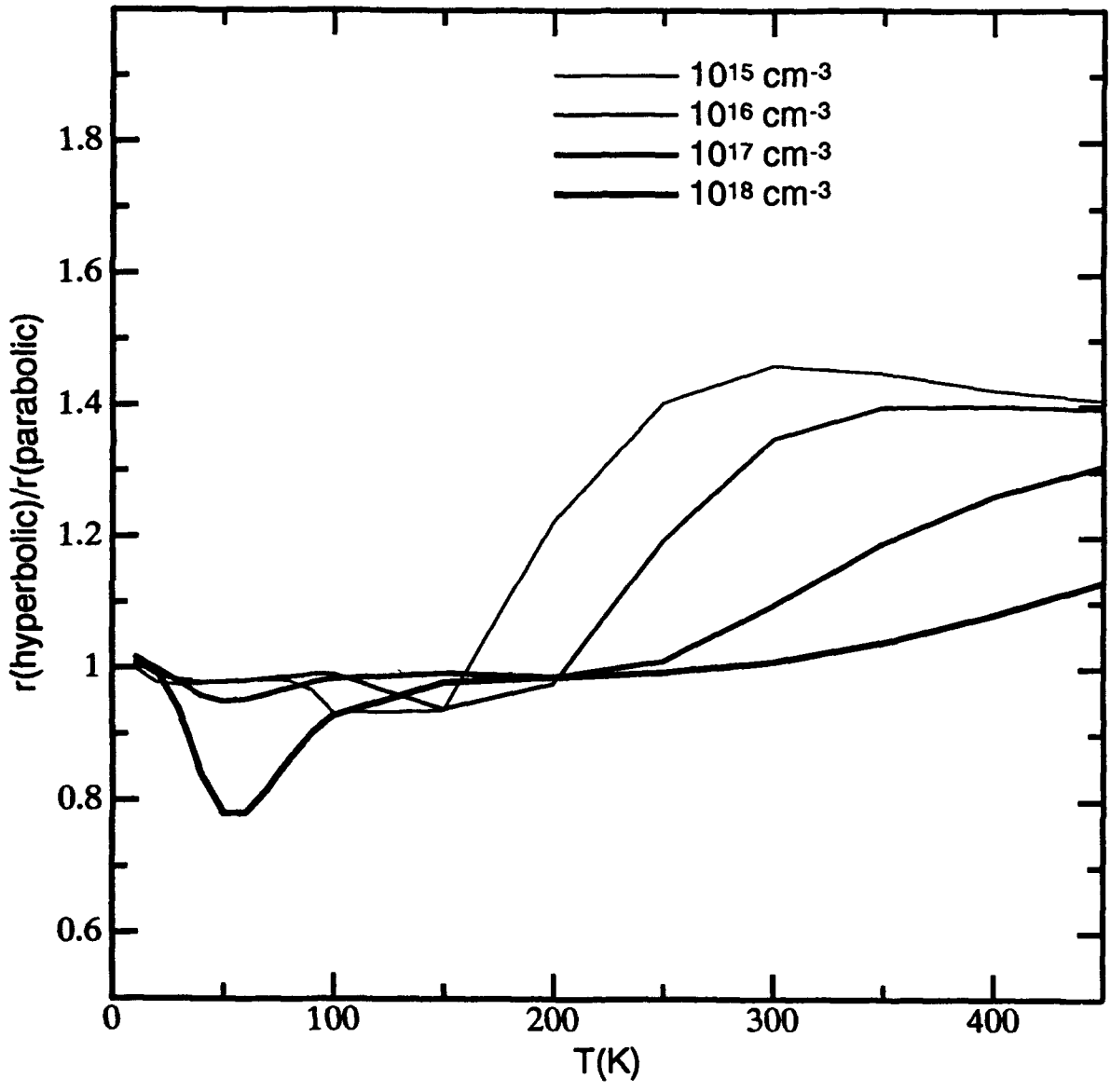

Figure 6 Hall factor as a function of temperature: HgZnTe

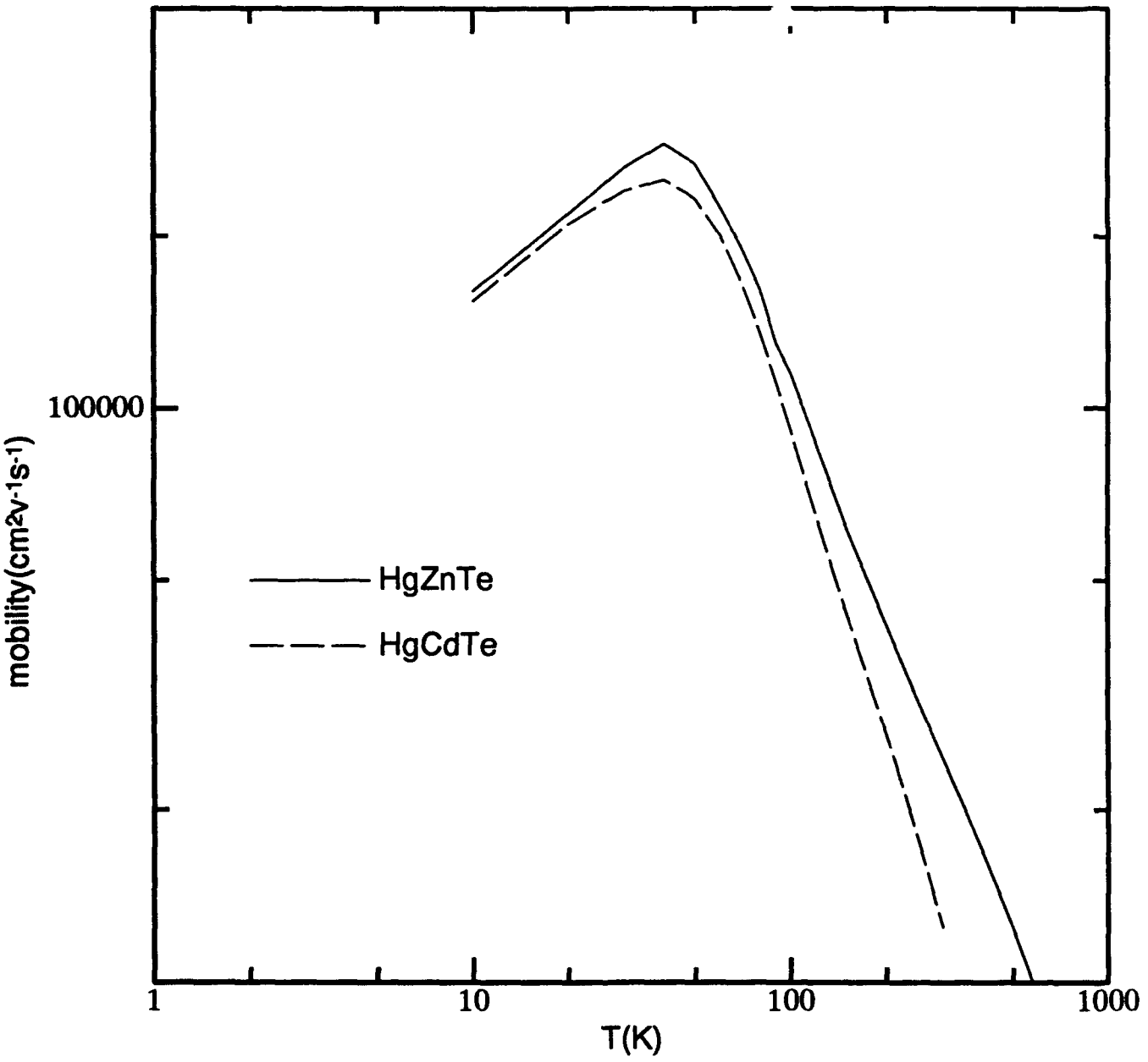

Figure 7 Electron Mobility

solution to BTE (Krishnamurthy and Sher, 1993). Thus, the calculated mobility with our hyperbolic band structure and usual k·p band structure is shown along with that obtained in collision time approximation and compared with values in HgCdTe in Figure 7.

One important feature of Figure 7 is that the hump in mobility near 40 K could be explained with competing impurity and phonon scattering rates. A hump in mobility is HgCdTe is seen experimentally. Also note that the mobility in HgZnTe is about 10-20% higher than in HgCdTe.

3.6 CONCLUSIONS

We have studied the effect of various approximations on electron transport coefficients and on ways to extract physical parameters from experiments. We point out how the values interpreted from experiments depend crucially on various approximations such as effective mass, MB statistics, and collision time. The main results are

- Approximating the Hall factor by unity over a wide range of carrier concentrations is accurate only for low temperatures, typically less than 100 K. An error of about 50% is expected at high temperatures and low carrier concentration (10^{15} cm^{-3}), and about 20% is expected at low T and high carrier concentration (10^{18} cm^{-3}).
- The mobility calculations with full solution to BTE with FD statistics predict a hump near 40 K. The mobility in HgZnTe is about 10-20% higher than that in HgCdTe.

4. WORK PLANNED

In the next quarter we will continue the calculation of the ionization energies of the defects in CdTe, ZnSe, and HgCdTe and the incorporation of these energies into the quasichemical formalism to predict densities of the ionized defect concentrations. We will continue the refinement of the calculation of the tellurium antisite mercury vacancy defect pair. We will present several papers at the MCT Workshop in October, and will be preparing for these presentations.

REFERENCES

Bartoli, F.J., J.R. Meyer, R.E. Allen, and C.A. Hoffman, 1982: J. Vac. Sci. Technol. **21**, 241.

Berding, M.A., S. Krishnamurthy, A. Sher, and A.-B. Chen, 1987: J. Vac. Sci. Technol. **A 5**, 3014.

Chen, A.-B., and A. Sher, 1981: Phys. Rev. B **23**, 5360.

Kane, E.O, 1957: J. Phys. Chem. Solids **1**, 249.

Krishnamurthy, S., A. Sher, and A.-B. Chen, 1987: J. Appl. Phys. **61**, 1475.

Krishnamurthy, S., A. Sher, and A.-B. Chen, 1986: Phys. Rev. B **33**, 1026.

Krishnamurthy, S., and A. Sher 1993: J. Appl. Phys. **75**, 7904.

Meyer, J.R., and F.J. Bartoli, 1982: J. Vac. Sci. Technol. **21**, 237.

Schmidt, J.L., 1970: J. Appl. Phys. **41**, 2876.

Sher, A., D. Eger, A. Zemel, H. Feldstein, and A. Raizman, 1986: J. Vac. Sci. Technol. A **4**, 2024.

Sze, S.M., 1981: *Physics of semiconductor devices* (Wiley, New York), p. 22.